JOURNAL OF MATERIALS SCIENCE 31 (1996) 5385–5389

Dependence of giant magnetoresistance on microstructures in ion-beam co-sputtered Co_xAg_{1-x} granular films

H. SANG, N. XU, S. Y. ZHANG, J. H. DU, Q. LI, Y. W. DU
National Laboratory of Solid State Microstructures and Institute for Solid State Physics, Nanjing University, and Center for Advanced Studies in Science and Technology of Microstructures, Nanjing 210093, People's Republic of China

A number of structural analysis methods were employed to investigate the microstructures of ion-beam co-sputtering of Co_xAg_{1-x} ($0 \leqslant x \leqslant 100$ at%) granular films. For $x = 22$ at%, the sample which has the optimal giant magnetoresistance at room temperature, there exists either crystallized or highly disordered regions shown by high-resolution electron microscopy. At the boundary between cobalt granules and the silver matrix, lattice mismatch was formed, leading to roughness of the interfaces. X-ray diffraction and transmission electron microscopy revealed that the samples had f c c structure at low x, with (1 1 1) texture, and the h c p structure gradually appeared as $x > 75$ at%. Relative lattice expansion was observed as x increased.

1. Introduction

Since Baibich *et al.* [1] first reported the effect of giant magnetoresistance (GMR) in Fe/Cr magnetic multilayers in 1988, the effect has also been observed in many other multilayers (e.g. Co/Cu, Co/Ag, Fe/Cu, etc.) [2–4] due to antiferromagnetic coupling of ferromagnetic layers separated by non-magnetic spacers. A few years later, Xiao *et al.* [5] and Berkowitz *et al.* [6] individually reported the same effect in non-multilayer magnetic systems. This reveals that the GMR effect is not unique to magnetic multilayer systems and can be observed easily in nanostructured granular systems in which magnetic granules are inhomogeneously embedded in a non-magnetic matrix. It is not surprising to observe the GMR effect in magnetic granular systems because some of the sputtered magnetic multilayers with GMR display the typical granular structured characteristics (e.g. Co/Cu) [7, 8]. The effect of GMR has potential applications for magnetic sensors and read-heads [9] and is helpful in understanding the fundamental mechanism of magnetotransport characteristics in magnetic inhomogeneous systems. Meanwhile, these systems can be easily prepared with various techniques and thermal treatment. Thus, great interest has focused on the study of the GMR effect in these systems.

In binary immiscible magnetic granular systems, single-domain magnetic granules with nanoscale size, a few to a few tens of nanometres, are formed due to phase separation and nucleating growth [10, 11]. Without an applied field, the magnetic moments of magnetic granules are highly random and the systems display high resistivity. In an applied field, there is a marked drop of resistivity due to the tendency of the highly random moments of magnetic granules aligned along the orientation of external field. Experimental investigations show that GMR strongly depends on the application of an external magnetic field, the size of the magnetic granules, the fabrication procedure and annealing treatment. The values of GMR in magnetic granular systems rival the magnitude of that in magnetic multilayers and often appear in a narrow range of concentrations of magnetic element. Its optimal values were often observed after proper annealing treatment [12–20].

Compared with experimental investigations, the theoretical approach to GMR in magnetic granular system has not yet been well established. Although there is a lack of general theoretical models to understand the origin of GMR in nanostructured magnetic granular system, it is believed that GMR originates from spin-dependent scattering of conducting electrons off ferromagnetic granules (bulk/interfaces) and the interfacial scattering is dominant due to the roughness and moment configuration of interfaces based on some phenomenological models [21–23]. Thus, intensive investigation on microstructures is important to interpret the mechanism of GMR in magnetic granular system theoretically.

In this paper, we report a systematic investigation of characteristics of microstructures in ion-beam co-sputtered Co_xAg_{1-x} granular films in order to reveal the dependence of GMR on microstructures. This may be helpful to understand the origin of GMR in this system.

2. Experimental procedure

The sample was prepared by the ion-beam co-sputtering technique. The high-vacuum system was equipped with a Kaufman ion gun in which the argon (99.99%)

0022–2461

pressure was 0.2 m torr (1 torr = 133.322 Pa). After being ionized in a high-voltage chamber, the argon ion beam, with energy 1.2 keV, was drawn by an accelerated grid and bombarded directly on to the water-cooled target at an incident angle of 45°. The target consisted of pure silver and cobalt, and small square cobalt pieces were adhered to the silver plate. Because of the different sputtering ratios of both cobalt and silver, the cobalt concentration could be adjusted by the number of cobalt squares and by the different patterns of these small pieces on the silver plate. The sputtered products were deposited on to substrates fixed on the water-cooled substrate holder installed at the specularly reflected direction, to obtain the maximum deposited ratio. The distances from the target to both ion gun and substrate holder were about 15 cm.

A series of samples was deposited on common glass substrates with thickness of the order of 400 nm at different substrate temperatures ($T_S = 300$ and 400 K). The cobalt concentration, x, was determined using an electron microprobe. The characteristics of the microstructure and phase separation in these samples were checked using a number of structural analysis methods. The conventional four-terminal method was employed to measure GMR of these samples in an applied magnetic field up to 11.2 kOe. All measurements reported here were made at room temperature.

3. Results and discussion

A series of Co_xAg_{1-x} samples was fabricated in the range $0 \leqslant x \leqslant 100$ at % at different substrate temperatures, T_S. The structures of these samples were investigated by X-ray diffraction (XRD), transmission electron microscopy (TEM), ferromagnetic resonance (FMR), and high-resolution electron microscopy (HREM).

Fig. 1 shows XRD patterns of these samples prepared at $T_S = 300$ K, illustrating the effect of cobalt concentration. These patterns exhibit fcc structure up to $x \leqslant 54$ at % attributable to peaks (1 1 1), (2 0 0), (2 2 0), and (3 1 1) planes of silver. Although there is a strong tendency for phase separation in the CoAg granular system, no crystallographic evidence of either fcc or hcp cobalt is found at low cobalt concentration ($x = 0$, 8 at %). This may be due to overlapping of both Co(1 1 1) and Ag(2 0 0) reflections. As x increases, the Ag(2 0 0) peak decreases to become a slight shoulder first (at $x = 13$, 22 at %) and then gradually increases with its FWHM expansion (from $x > 22$–54 at %), indicating high phase separation, formation and aggregation of small-sized cobalt granules, and thus enhancement of reflections of the Co(1 1 1) plane. The position of the Ag(2 0 0) [Co(1 1 1)] peak visibly shifts towards that of Ag(1 1 1), indicating either Co–Ag demixing or strain from coherent cobalt/silver interfaces. In addition, the Ag(2 0 0) peak gradually decreases with both full-width at half-maximum (FWHM) expansion and slightly vertical shift, and the Ag(3 1 1) peak has the similar tendency with variation of cobalt concentration, x. Finally, Ag(2 2 0) and Ag(3 1 1) peaks vanish at $x = 40$ at %. With continuous increase of x, the hcp structure of cobalt appears ($x \geqslant 75$ at %). The XRD patterns exhibited in Fig. 1 are cobalt concentration-dependent and reveal that these samples have preferential orientation with their (1 1 1) axes out-of-plane ($x \leqslant 54$ at %), which are different from that for the samples prepared at $T_S = 400$ K [24], indicating that the fabrication process of samples plays an important role and influences the microstructure of different samples.

A typical bright-field micrograph for as-deposited $Co_{22}Ag_{78}$ sample is presented in Fig. 2. It shows the obvious characteristics of granules. It can be seen that cobalt granules are inhomogeneously dispersed in the silver matrix with various shapes, due to the low concentration of cobalt. Most of them are roughly spherical, some look elongated, some ramified, some like cobblestones. The size of the cobalt granules shows a finite distribution ranging from a few to more than 20 nm with an average size of the order of 10 nm [25]. Fig. 3 shows electron diffraction patterns for $x = 8$ and 40 at % as-deposited samples. It reveals the polycrystalline structure of the samples and five reasonably sharp diffraction rings can be observed, which are close to the diffraction rings of fcc silver. No cobalt diffraction ring appears. The two electron diffraction patterns are joined along a diameter A–A so that the relative lattice expansion can be seen clearly

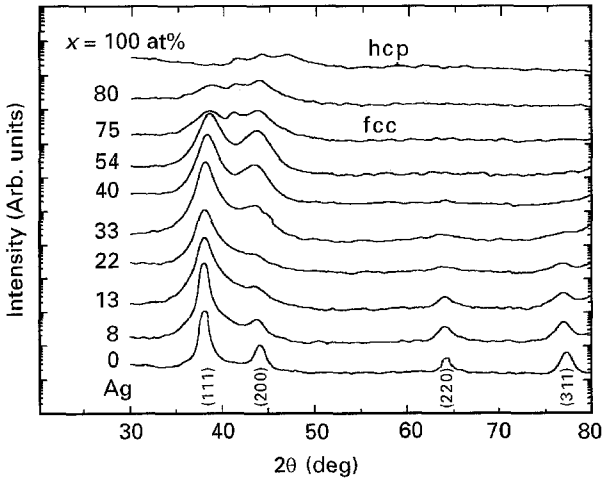

Figure 1 X-ray diffraction patterns for as-deposited Co_xAg_{1-x} film samples ($T_S = 300$ K) as a function of cobalt concentration, x.

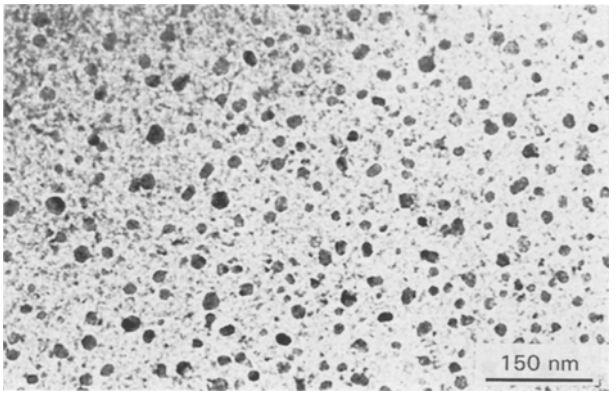

Figure 2 A typical bright-field micrograph of as-deposited $Co_{22}Ag_{78}$ sample.

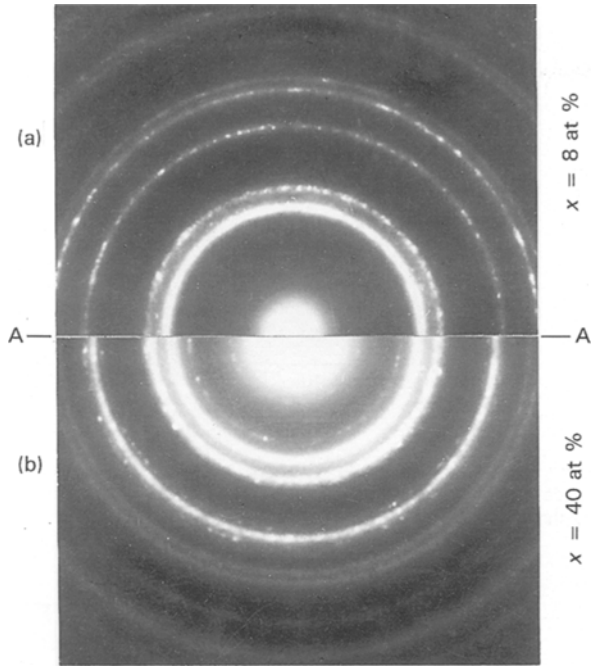

Figure 3 Electron diffraction patterns for two as-deposited CoAg samples ($T_S = 300$ K) of (a) $x = 8$ at % and (b) $x = 40$ at %. The relative lattice expansion can be seen along the diameter A–A.

from the difference in radii of corresponding diffraction rings as x increases. The d spacing of Ag(1 1 1) and (2 2 0) for the $x = 8$ at % sample is less than that for $x = 40$ at %. The diffraction rings of $x = 8$ at %, except the first ring (corresponding to Ag(1 1 1)), consist of intermittent bright spots, indicating the existence of grains with either worse quality of crystallinity or preferential orientation in the sample. For the $x = 40$ at % sample, all diffraction rings are continuous, and the second ring becomes broadened and bright due to the overlap of Co(1 1 1) and Ag(2 0 0). The increasing intensity of the second ring suggests that the high degree of crystallinity and phase separation are enhanced with increasing of cobalt concentration.

The HREM images for the $x = 22$ at % sample are shown in Fig. 4. Two kinds of morphological regions can be seen in Fig. 4a. A and B indicate the crystalline and highly disordered regions, respectively. Also in the same figure, there exists short-range ordering in the region indicated by B. The area indicated by black arrows is a cobalt granule about 4 nm in size with a two-dimensional lattice image of f c c cobalt oriented along the [1 1 1] direction, embraced by the disordered regions with an obscured boundary. Fig. 4b shows the connection of cobalt granules to the silver matrix with a size of more than 10 nm. The upper and lower parts correspond to cobalt and silver, respectively. The crystallographic planes of Co(2 0 0) connect with those of Ag(2 0 0). At the boundary, every five silver fringe connects with every six cobalt fringe to form a Moiré pattern due to the different crystallographic d spacings of cobalt and silver, leading to lattice mismatch [26, 27]. Because there is often a large distortion in the interfaces between cobalt granules and the silver matrix for as-deposited samples, a clear boundary of magnetic granules is hard to acquire. It is expected that further study using HREM will allow the atomic lattice images to be more clearly discerned for annealed samples.

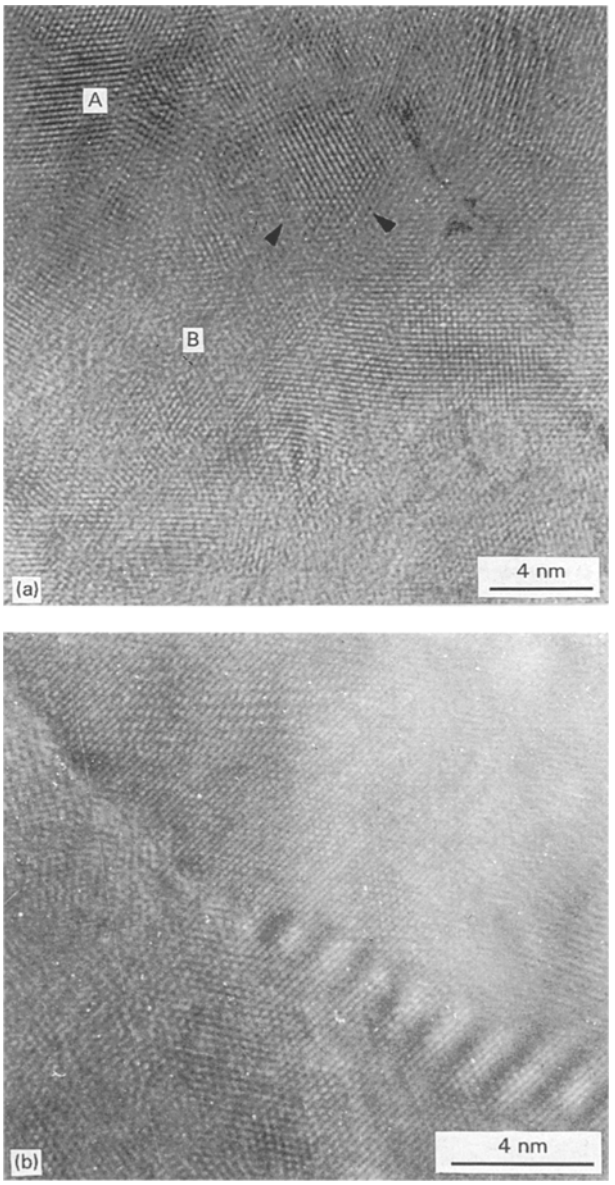

Figure 4 High-resolution electron microscope images of $Co_{22}Ag_{78}$ sample. (a) A and B indicate the regions of crystalline and high disorder, respectively. Black arrows indicate the two-dimensional image of a cobalt granule. (b) The connection between a cobalt granule and silver with a clear interface. The upper part is cobalt granule and lower part is silver.

Compared with two-dimensional morphological images obtained from TEM, as is well known, FMR can give three-dimensional information about the shapes of ferromagnetic granules. The FMR spectra were measured at room temperature. In the procedure, the microwave field was applied in the planes of samples with a frequency of 9.8 GHz. Fig. 5 presents the changes of uniform resonance field as function of x. In the figure, $H_\perp$ and $H_\parallel$ denote the applied d.c. field perpendicular and parallel to the sample plane, respectively. Below $x = 22$ at %, no resonance behaviour has been obtained due to low cobalt concentration, the coexistence of the regions of both worse quality of crystallinity and high disorder, being discerned from Fig. 3a, and the small size of magnetic granules. At $x = 22$ at %, $H_{r\perp} \approx H_{r\parallel}$, the difference in

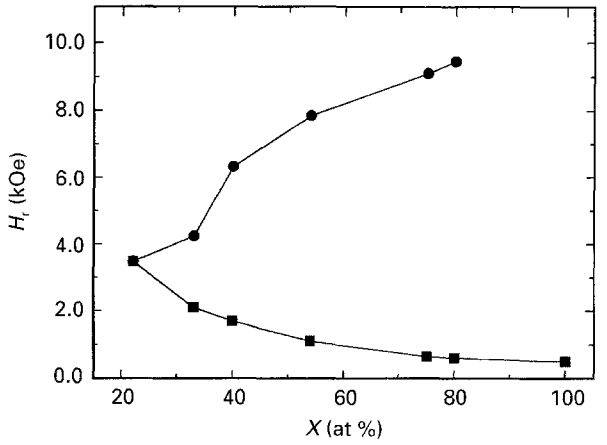

Figure 5 The dependence of uniform resonance field on cobalt concentration, x, in CoAg samples. (●) $H_\perp$ and (■) $H_\parallel$ are the applied d.c. fields perpendicular and parallel to the sample plane, respectively. Solid lines were drawn for the guide of eyes. $\omega = 9.8$ GHz, $T_S = 300$ K.

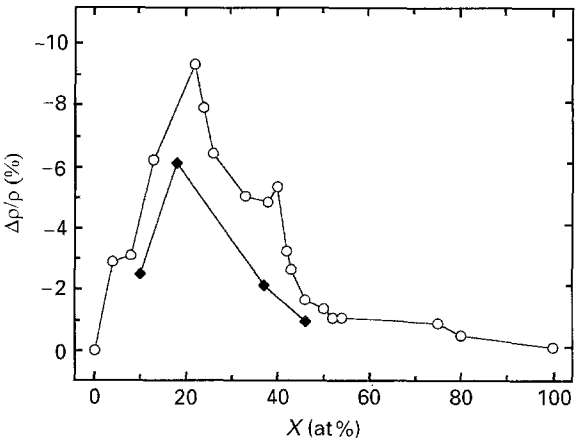

Figure 6 MR $\Delta\rho/\rho$ measured at room temperature versus cobalt concentration in Co_xAg_{1-x} samples prepared at different T_S: (○) 300 K, (◆) 400 K. $H = 11.2$ kOe.

resonance field increases monotonically as x increases, $\Delta H_r = H_{r\perp} - H_{r\parallel} \approx 0$ at $x = 22$ at % and ≈ 8.9 kOe at $x = 80$ at %, respectively. In term of the famous Kittel relation [28], it shows that cobalt granules were embedded in the silver matrix with roughly spherical shape at lower x. As x increases, small cobalt granules grow larger and aggregate into a network with large aspect ratio, thus leading to ΔH_r increases due to the shape-induced anisotropy.

Magnetoresistance was measured using the conventional four-terminal method in an applied field. The magnetoresistance ratio (MR), $\Delta\rho/\rho$, was calculated according to $\Delta\rho/\rho = [\rho(H) - \rho(0)]/\rho(0)$ where $\rho(0)$ and $\rho(H)$ are the resistivity in the initial zero field and external field H, respectively. Fig. 6 illustrates the values of $\Delta\rho/\rho$ versus cobalt concentration x for as-deposited samples prepared at different T_S measured with the current in plane and vertically applied magnetic fields. All the values of $\Delta\rho/\rho$ in Fig. 6 were measured at $H = 11.2$ kOe and were not saturated in this field. The curve of $\Delta\rho/\rho$ versus x clearly shows that $\Delta\rho/\rho$ first rises rapidly for $x \leqslant 22$ at % and reaches its maximum, as large as -9.3%, for $x = 22$ at %, and then it falls smoothly as x continuously increases for the as-deposited samples prepared at $T_S = 300$ K. The $\Delta\rho/\rho$ of these samples is larger than that of the samples prepared at $T_S = 400$ K. After annealing for 0.5 h at various T_A for the selected sample with $x = 22$ at %, which had the maximum $\Delta\rho/\rho$ in the as-deposited state, the optimal $\Delta\rho/\rho$ was found to become as large as -13.4% at $T_A = 500$ K, of which there was a 44% increase as compared with the as-deposited state. Fig. 7 shows the relation of GMR to external magnetic field for both as-deposited and annealed ($T_A = 500$ K) samples (Fig. 7a). The magnetization curve (Fig. 7b) was measured using a vibrating sample magnetometer (VSM) for as-deposited $Co_{22}Ag_{78}$ sample. It is clearly visible that, in the present field, GMR is not saturated for as-deposited and annealed samples. The behaviour of magnetization is typically supermagnetic at room temperature, and not saturated in the applied field up to 13.5 kOe,

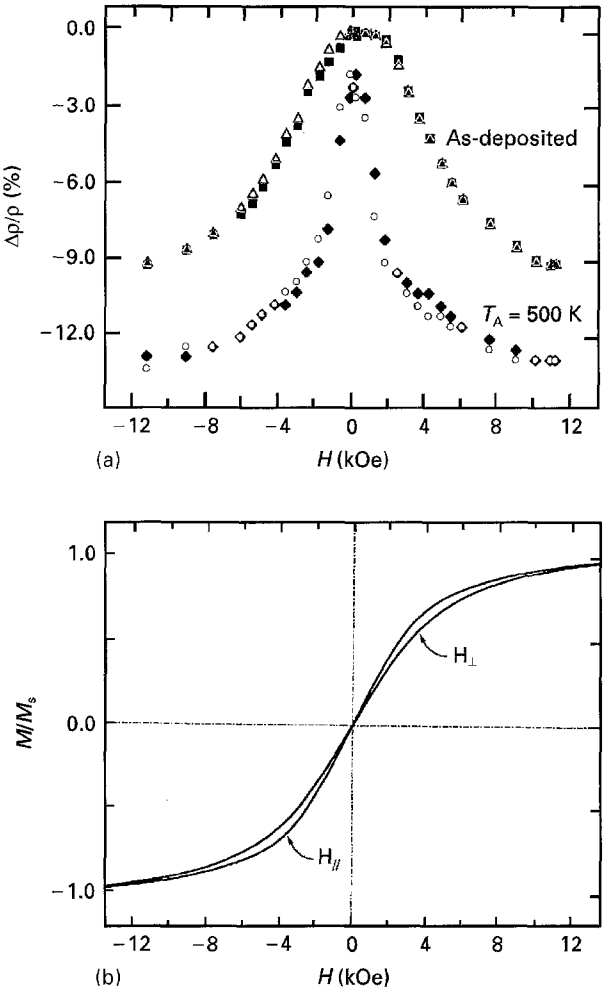

Figure 7 (a) MR as a function of external field for both as-deposited and annealed $Co_{22}Ag_{78}$ samples: (■) and (◆) correspond to field sweep from $-H$ to H, (△) and (○) mean the opposite. (b) Magnetic hysteresis loops for as-deposited $Co_{22}Ag_{78}$ sample. $H_\parallel$ and $H_\perp$ are the external fields parallel and perpendicular to the plane of the sample, respectively.

due to the contribution of the configuration of magnetic moments on the surfaces of the cobalt granules. In Fig. 7b, $H_\perp$ and $H_\parallel$ denote the external field perpendicular and parallel to the sample plane, respectively. The difference of the two loops with the external field

indicates that the easily magnetized axis is along the plane.

In terms of the binary phase diagram of Co–Ag alloy in the equilibrium solid state, the mutual solubility of cobalt and silver can be wholy negligible. Cobalt easily forms granules, embedded in the silver matrix as scattering centres, on adjusting both chemical compositions. With zero field, magnetic moments are highly randomly oriented and the systems display high resistivity. In an applied field, the marked drop of resistivity strongly depends on the orientation of magnetic moments. At low x, magnetic granules are so small that it is difficult to align the magnetic moments along the applied field. For $x = 22$ at %, cobalt granules grow rather large with an abundance of surfaces, leading to a larger surface/volume ratio and enhancing spin-dependent scattering; GMR results in its maximum value. It is, however, still unsaturated in a finite applied field due to the complex microstructures of the sample and the configuration of moments on the surfaces of the magnetic granules. After the correct annealing treatment, the structure of the interface between magnetic granules and the non-magnetic matrix is improved, leading to optimal GMR. As x increases, cobalt granules increase and tend to connect with each other to form bigger ones or chains until a network is formed, thus inducing the drastic decrease of GMR.

4. Conclusion

We have systematically investigated microstructures in Co_xAg_{1-x} granular films prepared using an ion-beam co-sputtering technique at different substrate temperatures. We have observed an optimal room-temperature GMR ratio as large as -9.3% for the as-deposited sample prepared at $T_S = 300$ K and -13.4% after annealing for 0.5 h at $T_A = 500$ K for the $x = 22$ at % sample. From the results of TEM, electron diffraction, and XRD patterns, the samples are found to display fcc structure ($x \leqslant 54$ at %) and hcp structure ($x > 75$ at %), and lattice expansion is observed as x increases. HREM observation shows the coexistence of crystalline and highly disordered regions in the as-deposited $Co_{22}Ag_{78}$ sample. The results reveal the dependence of GMR in Co_xAg_{1-x} granular films on cobalt concentration, annealing treatment, and external field. The dependence of GMR on microstructures has also been discussed.

Acknowledgements

We thank X. N. Zhao and J. M. Hong for their assistance in TEM measurements, and S. Y. Han and Y. X. Sui for their assistance in measurement of FMR spectra and for valuable discussions. This work was supported in part by Grants 85-6 NMS, NSFS, and JSNSF.

References

1. M. N. BAIBICH, J. M. BROTO, A. FERT, F. NGUYEN VAN DAU, F. FETROFF, P. ETIENNE, G. CREUZET, A. FRIEDERICH and J. CHAZELES, *Phys. Rev. Lett.* **61** (1988) 2472.
2. S. S. P. PARKIN, Jr. BHADRA and K. ROCHE, *ibid.* **66** (1991) 2152.
3. W. P. PRATT Jr, S.-F. LEE, J. M. SLAUGHTER, R. LLOLOEE, P. A. SCHROEDER and J. BASS, *ibid.* **66** (1991) 3060.
4. F. PETROFF, A. BARTHELEMY, D. H. MOSCA, D. K. LOTTIS, A. FERT, P. A. SCHROEDER, W. P. PRATT Jr, R. LLOLOEE and S. LEQUIEN, *Phys. Rev. B* **44** (1991) 5355.
5. J. Q. XIAO, J. S. JIANG and C. L. CHIEN, *Phys. Rev. Lett.* **68** (1992) 3749.
6. A. E. BERKOWITZ, J. R. MITCHELL, M. J. CAREY, A. D. YOUNG, S. ZHANG, F. E. SPADA, F. T. PARKER, A. HUTTEN and G. THOMAS, *ibid.* **68** (1992) 3745.
7. A. R. MODAK, S. S. P. PARKIN and D. J. SMITH, *J. Magn. Magn. Mater.* **129** (1994) 415.
8. S. S. P. PARKIN, Z. G. LI and D. J. SMITH, *Appl. Phys. Lett.* **58** (1991) 2710.
9. R. L. WHITE, *IEEE Trans. Mag.* **28** (1992) 2482.
10. C. L. CHIEN, *J. Appl. Phys.* **69** (1991) 5267.
11. J. R. CHILDRESS and C. L. CHIEN, *ibid.* **70** (1991) 5885.
12. J. Q. XIAO, J. S. JIANG and C. L. CHIEN, *IEEE Trans. Mag.* **29** (1993) 2688.
13. G. XIAO, J. Q. WANG and P. XIONG, *ibid.* **29** (1993) 2694.
14. P. XIONG, G. XIAO, J. Q. WANG, J. Q. XIAO, J. S. JIANG and C. L. CHEN, *Phys. Rev. Lett.* **69** (1992) 3220.
15. J. Q. XIAO, J. S. JIANG and C. L. CHIEN, *Phys. Rev. B* **46** (1992) 9266.
16. G. XIAO, J. Q. WANG and P. XIONG, *Appl. Phys. Lett.* **62** (1993) 420.
17. A. TSOUKATOS, H. WAN, G. C. HADIJIPANAYIS and Z. G. LI, *ibid.* **61** (1992) 3059.
18. *Idem, J. Appl. Phys.* **73** (1993) 5509.
19. H. WAN, A. TSOUKATOS, H. WAN and G. C. HADIJIPANAYIS, *Phys. Rev. B* **49** (1994) 1524.
20. J. A. BARNARD, S. HOSSAIN, M. R. PARKER, A. WAKNIS and M. L. WATSON, *J. Appl. Phys.* **73** (1993) 6372.
21. S. ZHANG and P. M. LEVY, *ibid.* **73** (1993) 5315.
22. M. R. PARKER, J. A. BARNARD, D. SEALE and A. WAKNIS, *ibid.* **73** (1993) 5512.
23. J. Q. WANG and G. XIAO, *Phys. Rev. B* **49** (1994) 3982.
24. H. SANG, Z. S. JIANG, G. GUO, J. T. JI, S. Y. ZHANG and Y. W. DU, *J. Magn. Magn. Mater.* **140–144** (1995) 589.
25. H. SANG, S. Y. ZHANG, H. CHEN, G. NI, J. M. HONG, X. N. ZHAO, Z. S. JIANG and Y. W. DU, *Appl. Phys. Lett.* **67** (1995) 2017.
26. J. H. DU, Q. LI, L. C. WANG, H. SANG, S. Y. ZHANG, Y. W. DU and D. FENG, *J. Phys. Condens. Matter.* **7** (1995) 9425.
27. J. H. DU, Q. LI, L. C. WANG, H. SANG, S. Y. ZHANG, Y. W. DU and D. FENG, *Phys. Status Solidi* **151** (1995) 313.
28. C. KITTEL, *Phys. Rev.* **73** (1948) 155.

Received 31 May 1995
and accepted 24 April 1996